Int. J. Electrochem. Sci., 15 **(2020)** 5342 – 5351, doi: 10.20964/2020.06.43

International Journal of
ELECTROCHEMICAL
SCIENCE
www.electrochemsci.org

Preparation of High-capacity Carbon-coated Nickel Cobaltate Hollow Nanospheres Electrode for supercapacitors

Guohui Chen, Yi Yang, Yatang Dai, Wei Wang[*]

State Key Laboratory of Environment-friendly Energy Material, School of Materials Science and Engineering, Southwest University of Science and Technology, Mianyang, 621010, PR China.
[*]E-mail: w.wang@swust.edu.cn

Received: 7 February 2020 / *Accepted:* 27 March 2020 / *Published:* 10 May 2020

$NiCo_2O_4$ is a binary transition metal oxide with a spinel structure. It has higher theoretical specific capacitance, good cycle stability, lower cost, and environmental friendliness. In this paper, hollow silica microspheres were prepared by using carbon dioxide microspheres as templates. The physical characterization results of the materials show that the prepared nanospheres have a good hollow spherical structure. After the carbon coating, a very obvious carbon particle layer grows on the surface of the hollow sphere. Electrochemical test results show that the rate performance and cycle stability of the carbon-coated nickel cobaltate hollow microspheres have been significantly improved, and the charge transfer resistance has been significantly reduced. The specific capacitance reaches 637.5 F/g at a current density of 0.5 A/g. When the current density is changed from 0.5 A/g to 5 A/g, the capacitance retention is as high as 90.2%. At a current density of 5 A/g, the carbon-coated nickel cobaltate hollow microspheres can maintain a specific capacitance of 91.7% after 2000 charge and discharge cycles.

Keywords: $NiCo_2O_4$, carbon coating, hollow sphere, electrochemical performance

1. INTRODUCTION

As a kind of energy storage device, supercapacitor has good electrochemical performance and wide application, and its research has attracted much attention[1, 2]. As a supercapacitor electrode material , nickel cobaltate can undergo a rapid redox reaction during the electrochemical process and thus exhibit excellent Faraday pseudocapacitance characteristics[3-7]. Nevertheless, there are still several problems that have greatly impaired its electrochemical performance and limited the application of nickel cobaltate as an electrode material for supercapacitors [8, 9]. First, the poor intrinsic electron and ionic conductivity of nickel cobaltate is detrimental to full and rapid electrochemical ion diffusion and charge conversion. Secondly, the large amount of expansion and contraction during the charge and discharge process causes the destruction and aggregation of nickel cobaltate, which makes its poor

cycling performance and rate capability. Moreover, the low utilization rate of active nickel cobaltate has a negative impact on their practical application [10-13]. Therefore, the composite of carbon-based materials into nicke cobaltate is beneficial to the creation of a continuous conductive network and interpenetrating ion transmission paths throughout the electrode [14, 17]. It can not only improve the conductivity as a conductive agent, but also can be used as a physical buffer for the hollow structure of nickel cobaltate [18, 19]. At the same time, the material can be protected from structural degradation, thereby achieving maximum utilization to achieve high capacity and long cycle life [20].

An ideal material for composite carbon-based materials into nickel cobaltate is dopamine (DA), which contains two electrochemically active phenolic hydroxyl groups and one electrochemically active amino group in its molecule. Under weak alkaline conditions, dopamine hydrochloride will self-polymerize to form polydopamine [21, 22]. After carbonization, it can form a network structure similar to graphene [23]. This structure makes the carbon material have a larger specific surface area [24].

In this paper, carbon-coated nickel cobaltate hollow microspheres ($NiCo_2O_4$ HS@C) were prepared by template method using silica microspheres as template and polydopamine as carbon-based material [25] to form carbon-based material nickel cobaltate hollow spheres ($NiCo_2O_4$ HS). This paper also studies the change in the properties of the material before and after carbon coated.

2. EXPERIMENTAL

2.1. Chemicals

All reagents are analytical grade and can be used directly without further purification. $Co(NO_3)_2{\cdot}6H_2O$, $Ni(NO_3)_2{\cdot}6H_2O$, ethyl orthosilicate, ammonia, ethanol, hexamethylenetetramine and trimethylolaminomethane were purchased from Kelong Chemical Co. Ltd (Chengdu China), and dopamine hydrochloride was obtained from Aladdin Co., Ltd. (Shanghai, China)..

2.2. Preparation of SiO_2 nano-microspheres

Stöber method was used to prepare silica nanospheres [26]. In a typical experiment, 4.5 ml ethyl orthosilicate was added in 24.75 ml deionized water and 67.75 ml ethanol mixed solution. Then, 3 ml ammonia was added dropwise and stirring at 25 ° C for 2 hours to obtain silica nanospheres.

2.3. Preparation of $NiCo_2O_4$ HS

SiO_2@$NiCo_2O_4$ precursor was prepared by a liquid-phase precipitation method[27], and then $NiCo_2O_4$ HS was obtained by etching and calcination from the precursor. In a typical synthesis, 11 mmol silica nanospheres were dispersed in 50 ml deionized water, then 0.388 g $Co(NO_3)_2{\cdot}6H_2O$ and 0.194 g $Ni(NO_3)_2{\cdot}6H_2O$ were added. After sonicated for 0.5 h, 1.869 g hexamethylenetetramine was dissolved under the condition of magnetic stirring. Then, the mixture was refluxed at 90 °C for 6 h. After

centrifugal, the precipitate of SiO_2@$NiCo_2O_4$ precursor was collected and dried in a vacuum oven at 25 °C over night.

After dispersing the precipitate in 50 ml deionized water, 22 mmol of NaOH was added in the solution, and magnetically stired for 15 minutes. The solution was then transferred to a hydrothermal reactor and reacted at 160 °C for 12 hours. After cooling to room temperature, the solution was centrifuged and washed by ethanol and deionized water at least 3 times. Finally, the product was put into a tube furnace, and the temperature was raised to 300 °C at a increasing rate of 1 °C/min. After calcined for 2 hours, the $NiCo_2O_4$ HS was obtained.

2.4. Preparation of $NiCo_2O_4$ HS@C

In a typical synthesis, 40 mg prepared $NiCo_2O_4$ HS was dispersed in 20 ml deionized water, then 24 mg trimethylolaminomethane was dissolved in the solution. After sonicated for 30 minutes, 20 mg dopamine hydrochloride was added and stirred at room temperature for 10 hours. After the reaction, black product was obtained by centrifuge. After that, the product was carefully placed in a tube furnace, and the temperature was increased to 500 °C at a temperature rising rate of 5 °C/min under a nitrogen atmosphere. Finally, $NiCo_2O_4$ HS@C was obtained after calcining for 1 hour.

2.5. Electrochemical Characterization

All electrochemical tests were performed in an electrochemical workstation (CHI 660e Chenghua, Shanghai, China) . The prepared material was mixed and ground with poly(vinylidene fluoride) (PVDF) and acetylene black at a mass ratio of 7:2:1, and coated on the cleaned nickel foam sheet to prepare the required working electrode. A platinum electrode was used as the auxiliary electrode, Ag/AgCl was used as the reference electrode, and a 3 mol/L potassium hydroxide solution was used as the electrolyte. The main test methods are Cyclic Voltammetry (CV), electro-chemical impedance spectroscopy (EIS), and Galvanostatic charge-discharge (GCD). According to the constant current charge-discharge curve, use formula (1) to calculate Cs. According to the formula (2), the impedance of the electrode can be obtained by fitting the equivalent circuit diagram.

$$C = \frac{I \cdot t}{m \cdot \Delta V} \quad (1)$$

Where: I is the charge and discharge current, t is the discharge time, m is the mass of the active material, and ΔV is the potential window.

$$Z = R_{\Omega} + \frac{1}{jwC_d + \frac{1}{R_{ct}}} \quad (2)$$

Where: Z is the impedance of the electrode, R_{Ω} is the resistance of the solution, jwC_d is the admittance of pure capacitance, and R_{ct} is the charge transfer resistance.

2.6. Characterization of materials

The material composition of materials was studied by X-ray diffraction (XRD, DMAX1400). The morphology and microstructure of the products were characterized by field emission scanning electron microscopy (FSEM, Ultra 55) and transmission electron microscopy (TEM, 200FE Libra).

3. RESULTS AND DISCUSSION

3.1 Morphologies and structure of $NiCo_2O_4$ HS and $NiCo_2O_4$ HS@C

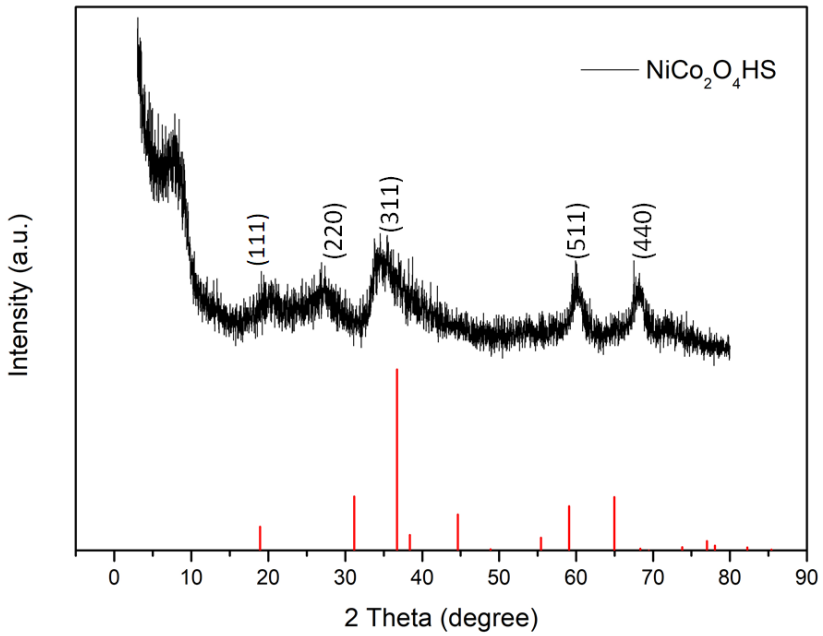

Figure 1. X-ray diffraction pattern of $NiCo_2O_4$ HS

Figure 1 is the X-ray diffraction pattern of $NiCo_2O_4$ HS. From the figure 1, the position of the peak basically meets the standard cobalt nickel nickel card PDF #73-1702. Obvious diffraction peaks appeared near 2θ angles of 18.928°, 31.151°, 36.704°, 59.113°, and 64.961°, and the corresponding crystal plane indices were (111), (220), (311), (511), and (440), respectively. It shows that the prepared material is $NiCo_2O_4$.

Figure 2 (a) is SEM image of SiO_2. The prepared silica microspheres have a good spherical structure which could provide a reliable template for the preparation of $NiCo_2O_4$ HS. Figure 2 (b) is a SEM image of $NiCo_2O_4$ HS prepared by the template method. From the figure, we can see that the prepared $NiCo_2O_4$ HS shows spherical structure with a size of about 500 nm. We can also see that there are a large number of nanosheets on the surface of $NiCo_2O_4$ HS, and these sheet-like structures greatly increase their specific surface area [28]. Moreover, the flaky stacking leads to $NiCo_2O_4$ HS a three-dimensional mesoporous structure [29], allowing the material to store more energy and make it have better electrochemical performance. Furthermore, we can clearly observed the partially damaged of $NiCo_2O_4$ HS, which proves that the $NiCo_2O_4$ HS are hollow structures.

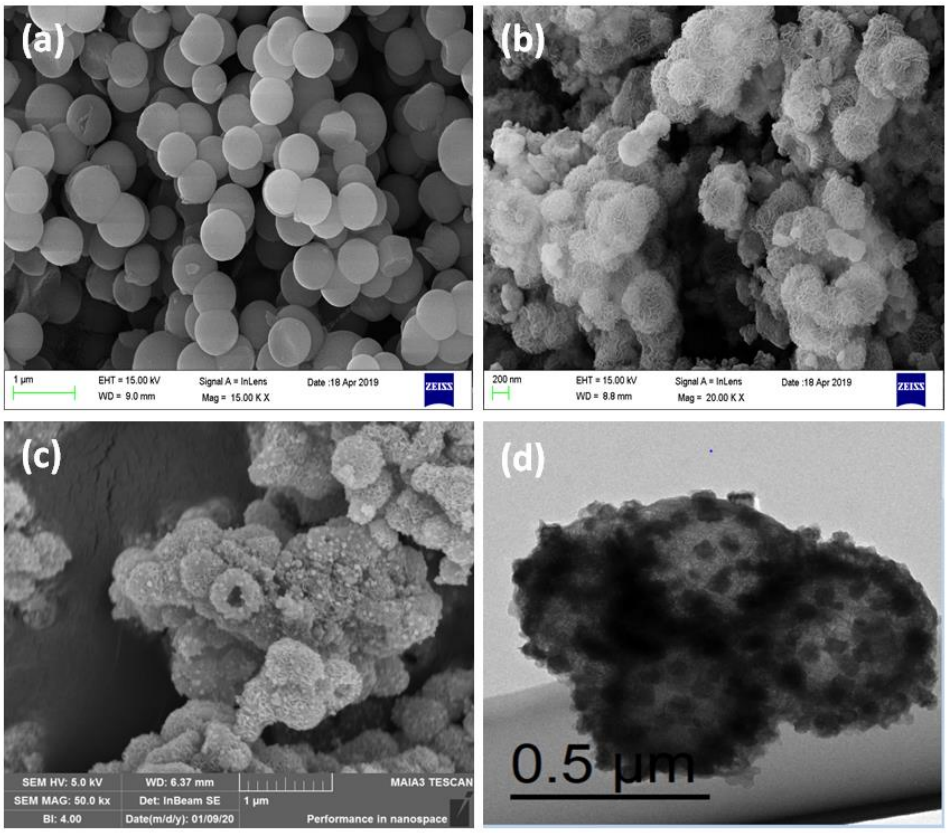

Figure 2. (a) SEM image of SiO_2, (b) SEM image of $NiCo_2O_4$ HS, (c) SEM image of $NiCo_2O_4$ HS@C, (d) TEM image of $NiCo_2O_4$ HS@C

Figure 2 (c) is a SEM image of $NiCo_2O_4$ HS@C. From the figure, we can see that the size of $NiCo_2O_4$ HS@C is about 500 nm. In addition, we can also see the carbon particles formed on the surface of the pellet. From the TEM image of $NiCo_2O_4$ HS@C, Figure 2 (d), we can clearly observe the hollow structure of $NiCo_2O_4$ HS@C. A large amount of granular carbon is also observed attaching on the surface of $NiCo_2O_4$ HS, which greatly improves the specific surface area of the $NiCo_2O_4$ HS@C. Moreover, the electrical conductivity of $NiCo_2O_4$ HS@C is enhanced due to the electroactive sites of the carbon layer [30].

3.2. Electrochemical Performance

Figure 3 is the CV curves of (a) $NiCo_2O_4$ HS and (b) $NiCo_2O_4$ HS@C at different scan rates. Compared with $NiCo_2O_4$ HS, $NiCo_2O_4$ HS@C has more pronounced redox peaks, which indicates that it has a greater redox reaction and exhibits more obvious pseudocapacitive characteristics. Comparing the cyclic voltammetry curves, it can be found that $NiCo_2O_4$ HS@C has a larger peak area, indicating its capacitance performance is also better than $NiCo_2O_4$ HS. With the increase of the scan rate, the oxidation and reduction peaks of $NiCo_2O_4$ HS@C shifted to both ends, respectively, but the overall trend of their shape and cycle remained basically unchanged, reflecting good rate performance and reversible performance.

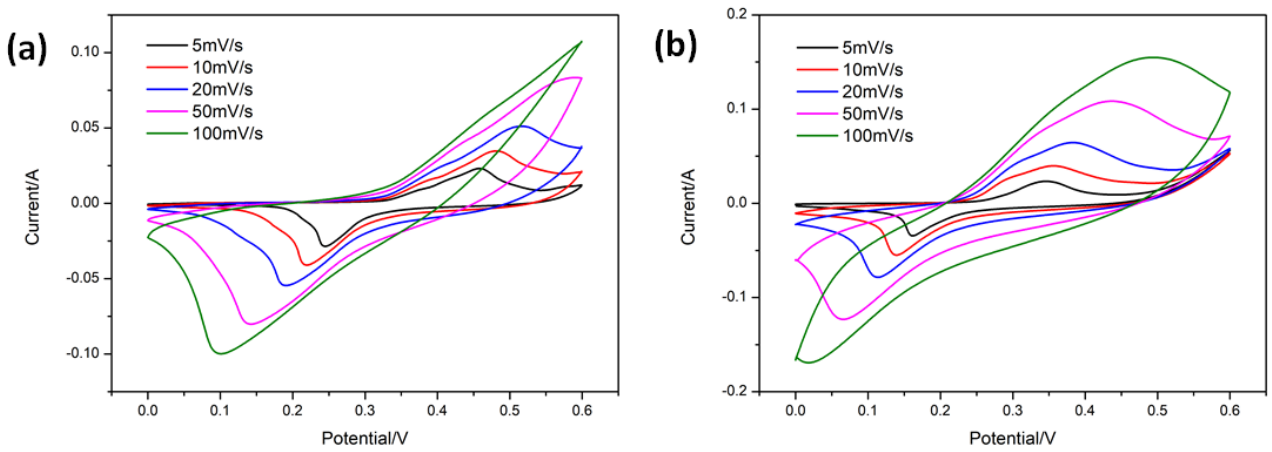

Figure 3. CV curves of (a) $NiCo_2O_4$ HS and (b) $NiCo_2O_4$ HS@C

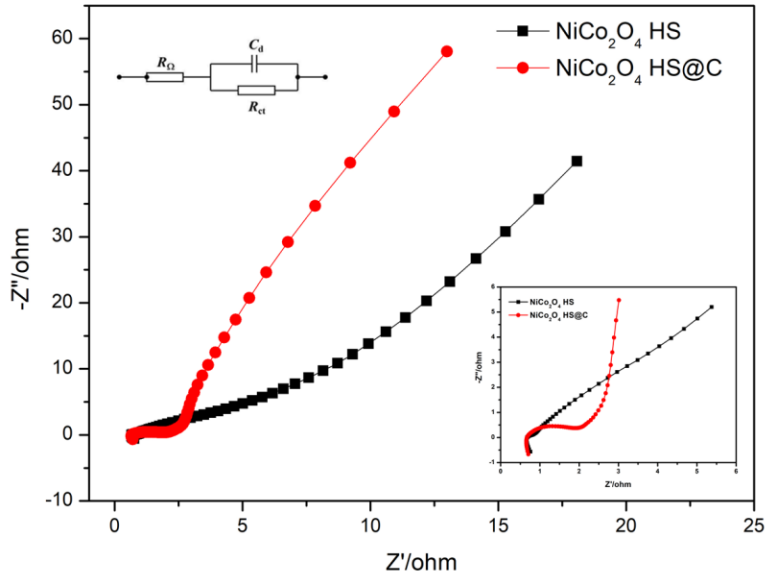

Figure 4. EIS curves of $NiCo_2O_4$ HS and $NiCo_2O_4$ HS@C

Figure 4 is the EIS curves of $NiCo_2O_4$ HS and $NiCo_2O_4$ HS@C. According to the data in the figure, the R_Ω of $NiCo_2O_4$ HS is 0.77262 Ω and the R_{ct} is 2.156Ω. $NiCo_2O_4$ HS@C has an R_Ω of 0.73047 Ω and an R_{ct} of 1.174 Ω. From the fitting results, the charge transfer resistance of these two materials is relatively small, both of them have good electrical conductivity. The comparison found that $NiCo_2O_4$ HS@C has a smaller charge transfer resistance and a significant improvement in performance. This is because the carbon material on the surface of $NiCo_2O_4$ HS@C has the advantage of high conductivity. In the figure, $NiCo_2O_4$ HS@C has a larger slope, indicating that its ion diffusion is faster and its performance is better than $NiCo_2O_4$ HS. The reason is that the coated carbon particle layer generates a continuous conductive network and interpenetrating ion transmission paths in the entire electrode, thereby improving the conductivity and ion diffusion rate of $NiCo_2O_4$ HS@C.

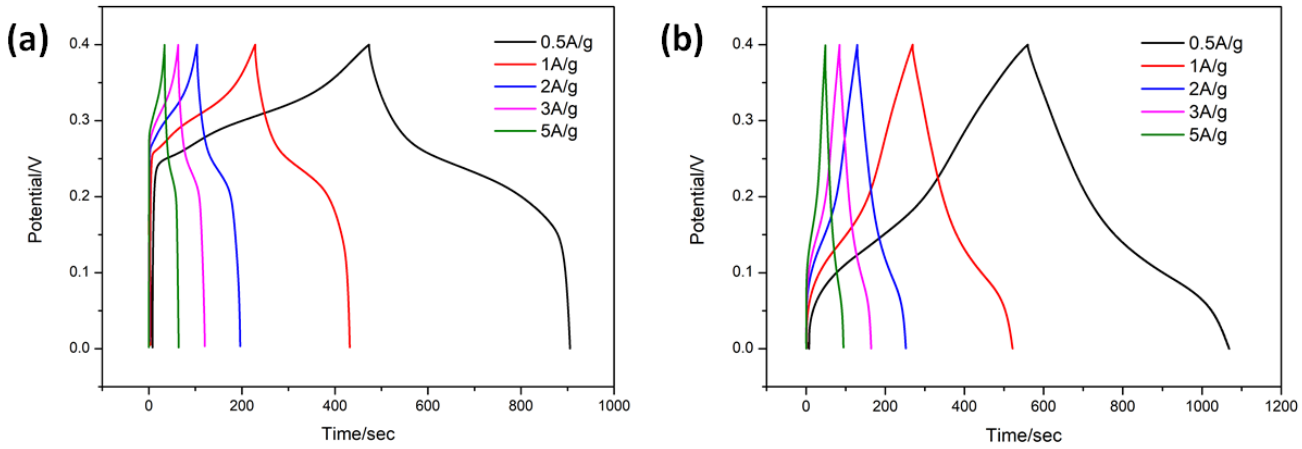

Figure 5.GCD curves of $NiCo_2O_4$ HS and $NiCo_2O_4$ HS@C

Figure 5 (a) and (b) are the GCD curves of $NiCo_2O_4$ HS and $NiCo_2O_4$ HS@C in different current densities. In Figure 5 (a), the charge-discharge performance was measured, and the charging time and the discharging time were basically the same. Moreover, they both show obvious charge and discharge platforms, and obvious pseudocapacitive characteristics. The results are consistent with the CV test of Figure 3 (a). The specific capacitances of $NiCo_2O_4$ HS at current densities of 0.5 A/g, 1 A/g, 2 A/g, 3 A/g, 5 A/g, are 541.25 F/g, 507.5 F/g, 470 F/g, 427.5 F/g, and 375 F/g, respectively. The specific capacitance of the $NiCo_2O_4$ HS decrease with the increase of the current density. From the curves of Figure 5 (b), we can also observe the obvious charge and discharge platform, which corresponds to the peaks in the CV test of Figure 3 (b). By calculation, we can conclude that at current densities of 0.5 A/g, 1 A/g, 2 A/g, 3 A/g, 5 A/g, the specific capacitances of $NiCo_2O_4$ HS@C are 637.5 F/g, 636.25 F/g, 615 F/g, 607.5 F/g, 575 F/g, respectively.

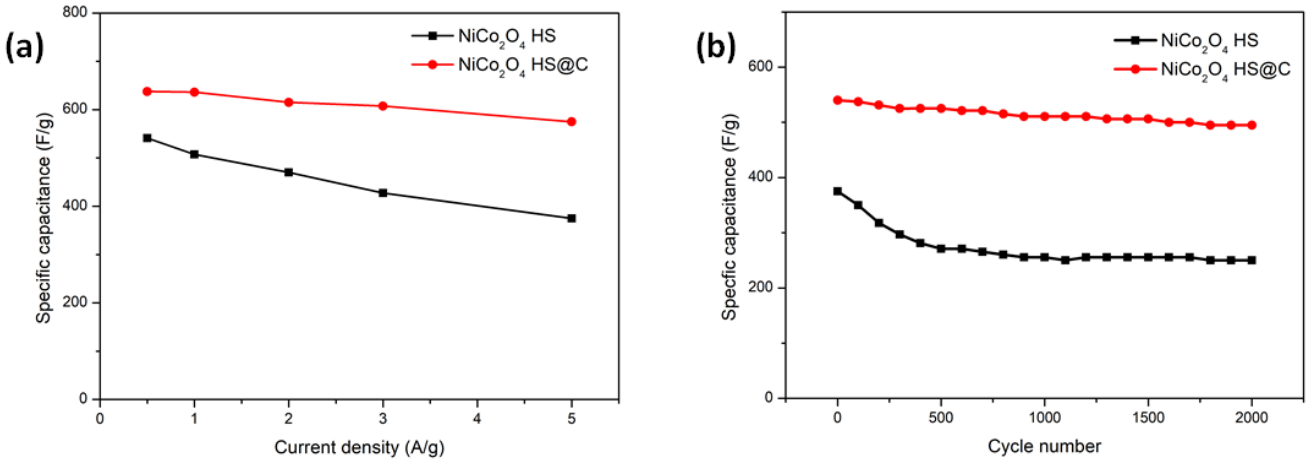

Figure 6. (a) Specific capacitances calculated from GCD curves, (b) Cyclic stability.

Figure 6 (a) is the specific capacitances calculated from GCD curves of $NiCo_2O_4$ HS and $NiCo_2O_4$ HS@C. The comparison shows that the capacitance performance of the $NiCo_2O_4$ HS@C has

been significantly improved, especially at a lower current density. When the current density was increased from 0.5 A/g to 5 A/g, the capacitance retention of $NiCo_2O_4$ HS was 69.3%, while the capacitance retention of $NiCo_2O_4$ HS@C was 90.2%. Figure 6 (b) is the cycle stability test of $NiCo_2O_4$ HS and $NiCo_2O_4$ HS@C. At a current density of 5 A/g, $NiCo_2O_4$ HS maintains a specific capacitance of 66.7%, $NiCo_2O_4$ HS@C has maintained a specific capacitance of 91.7% after 2000 charge-discharge cycle tests. This shows that the carbon layer can effectively improve the cycle life of the $NiCo_2O_4$ HS@C.

Table 1. Specific capacitance of $NiCo_2O_4$ with different morphologies

Material	Electrolyte	specific capacitance ($F\ g^{-1}$)	References
$NiCo_2O_4$NSs@HMRAs	1M KOH	678 (6A/g)	[3]
$NiCo_2O_4$ microspheres	6M KOH	192 (20A/g)	[15]
$NiCo_2O_4$ nanowires	2M KOH	471 (1A/g)	[20]
GE/$NiCo_2O_4$	1M KOH	591 (1A/g)	[24]
NCOs	1M KOH	453 ($5mV/s^{-1}$)	[28]
$NiCo_2O_4$ HS@C	3M KOH	636.25 (1A/g)	This study

NSs@HMRAs: nanosheets@hollow microrod arrays, GE: graphene-decorated
NCO: nickel–cobalt oxide

In addition, the specific capacitance of the $NiCo_2O_4$ HS @ C prepared separately is compared with other $NiCo_2O_4$ with different morphologies in the reference, as shown in Table 1. The results show that $NiCo_2O_4$ HS @ C has a higher specific capacity. The reason is that the prepared $NiCo_2O_4$ HS @ C has a three-dimensional mesoporous structure, which can increase the specific capacity of the material. Secondly, the formed granular carbon layer can effectively suppress the agglomeration of the material. The conductivity and specific constant of the material increase the specific capacity of the material.

4. CONCLUSIONS

In this paper, $NiCo_2O_4$ HS@C were prepared by using a template method with silica nanospheres as a template after etching and calcination. The electrochemical performance test results show that $NiCo_2O_4$ HS@C exhibits the characteristics of a pseudocapacitive characteristics, with a specific capacitance of 637.5 F/g at a current density of 0.5 A/g, which is significantly higher than $NiCo_2O_4$ HS

(541.25 F/g at 0.5 A/g). When the current density changes from 0.5 A/g to 5 A/g, its capacitance retention is as high as 90.2%. It can maintain a specific capacitance of 91.7% after 2000 charge-discharge cycles at a current density of 5 A/g, showing excellent electrochemical performance.

ACKNOWLEDGEMENTS
This research was supported by the project of State Key Laboratory of Environment-friendly Energy Material, Southwest University of Science and Technology(18FKSY0207, 17FKSY0113), Southwest University of Science and Technology Longshan Academic Talent Research Support Program (17LZX604).

References

1. G. Wang, L. Zhang, J. Zhang, *Chem. Rev.*, 41 (2012) 797.
2. F. Wang, X. Wu, X. Yuan, Z. Liu, Y. Zhang, L. Fu, Y. Zhu, Q. Zhou, Y. Wu, W. Huang, Chem. Soc. Rev., 46 (2017) 6816.
3. X. F. Lu, D. J. Wu, R. Z. Li, Q. Li, S. H. Ye, Y. X. Tong, G. R. Li, *J. Mater. Chem. A*, 2 (2014) 4706.
4. L. Wang, Y. Huang, X. Li, H. Ma, C. You, J. Liu, Y. Huang, Y. Hua, C. Wang, *Funct. Mater. Lett.*, 1 (2019) 1.
5. F. Yang, K. Zhang, W. Li, K. Xu, *J. Colloid Interface Sci.*, 556 (2019) 386.
6. Y. R. Zhu, P. P. Peng, J. Z. Wu, T. F. Yi, Y. Xie, S. Luo, *Solid State Ion.*, 336 (2019) 110.
7. Q. Sui, C. Xiang, Y. Zou, E. Yan, H. Zhang, F. Xu, L. Sun, *Int. J. Electrochem. Sci.*, 14 (2019) 10710.
8. C. Jun, Z. Jing, W. Y. Chi, *J. Inorg. Mater.*, 34 (2019) 121.
9. C. Ji, F. Liu, L. Xu, S. Yang, *J. Mater. Chem. A*, 5 (2017) 5568.
10. T. Wang, Y. Guo, B. Zhao, S. Yu, H. P. Yang, D. Lu, X. Z. Fu, R. Sun, C. P. Wong, *J. Power Sources*, 286 (2015) 371.
11. J. Wu, P. Guo, R. Mib, X. Liu, H. Zhang, J. Mei, H. Liu, W.-M. Lau, L. M. Liu, *J. Mater. Chem. A*, (2015) 2.
12. Y. L. Wu, W. Guo, X.J. Lian, Y.M. Tian, W.G. Wang, J.Y. Li, S. Wang, *J. Alloy. Compd.*, 793 (2019) 418.
13. Y. Liu, D. Zhao, H. Liu, A. Umar, X. Wu, *Chin. Chem. Lett.*, 30 (2019) 1105.
14. H. Zhang, D. Xiao, Q. Li, Y. Ma, S. Yuan, L. Xie, C. Chen, C. Lu, *J. Energy Chem.*, 27 (2018) 195.
15. L. Shen, Q. Che, H. Li, X. Zhang, *Adv. Funct. Mater.*, 24 (2014) 2630.
16. J. Du, L. Liu, Y. Yu, Y. Zhang, A. Chen, *Chin. Chem. Lett.*, 30 (2019) 1423.
17. H. Deng, M. Zhu, T. Jin, C. Cheng, J. Zheng, Y. Qian, *Int. J. Electrochem. Sci.*, 15 (2020) 16.
18. Z. Yang, F. Xu, W. Zhang, Z. Mei, B. Pei, X. Zhu, *J. Power Sources*, 246 (2014) 24.
19. D. Lan, M. Qin, J. Liu, G. Wu, Y. Zhang, H. Wu, *Chem. Eng. J.*, 382 (2020) 122797.
20. F. Deng, L. Yu, M. Sun, T. Lin, G. Cheng, B. Lan, F. Ye, *Electrochim. Acta*, 133 (2014) 382.
21. L. Ku, Y. Cai, Y. Ma, H. Zheng, P. Liu, Z. Qiao, Q. Xie, L. Wang, D. L. Peng, *Chem. Eng. J.*, 370 (2019) 499.
22. X. Yao, C. Zhao, J. Kong, D. Zhou, X. Lu, *RSC Adv.*, 4 (2014) 37928.
23. C. Peng, J. Yu, S. Chen, L. Wang, *Chin. Chem. Lett.*, 30 (2019) 1137.
24. B. Li, Q. Sun, R. Yang, D. Li, Z. Li, *J. Mater. Sci.-Mater. Electron.*, 29 (2018) 7681.
25. X. Zhang, Y. Zhou, B. Luo, H. Zhu, W. Chu, K. Huang, *Nano-Micro Lett.*, 10 (2017) 2.
26. S.L. Greasley, S.J. Page, S. Sirovica, S. Chen, R.A. Martin, A. Riveiro, J.V. Hanna, A.E. Porter, J.R. Jones, *J. Colloid Interface Sci.*, 469 (2016) 213.
27. K. Xu, J. Yang, J. Hu, *J. Colloid Interface Sci.*, 511 (2018) 456.

28. X. Lu, X. Huang, S. Xie, T. Zhai, C. Wang, P. Zhang, M. Yu, W. Li, C. Liang, Y. Tong, *J. Mater. Chem.*, 22 (2012) 13357.
29. Y. Li, L. Zou, J. Li, K. Guo, X. Dong, X. Li, X. Xue, H. Zhang, H. Yang, *Electrochim. Acta*, 129 (2014) 14.
30. L. Peng, Y. Ouyang, W. Li, H. J. Qiu, Y. Wang, *Electrochim. Acta*, 190 (2016) 126.